

PPPL-2321

25

PPPL-2321

UC20-F

PPPL--2321

DE86 011162

156
6/5/86 JS (2)

CHARGE-EXCHANGE AND FUSION REACTION MEASUREMENTS
DURING COMPRESSION EXPERIMENTS WITH NEUTRAL BEAM HEATING
IN THE TOKAMAK FUSION TEST REACTOR

By

R. Kaita et al.

APRIL 1986

PLASMA
PHYSICS
LABORATORY



PRINCETON UNIVERSITY
PRINCETON, NEW JERSEY

PREPARED FOR THE U.S. DEPARTMENT OF ENERGY,
UNDER CONTRACT DE-AC02-76-CO-3073.
DISTRIBUTION OF THIS DOCUMENT IS UNLIMITED

NOTICE

This report was prepared as an account of work sponsored by the United States Government. Neither the United States nor the United States Department of Energy, nor any of their employees, nor any of their contractors, subcontractors, or their employees, makes any warranty, express or implied, or assumes any legal liability or responsibility for the accuracy, completeness or usefulness of any information, apparatus, product or process disclosed, or represents that its use would not infringe privately owned rights.

Printed in the United States of America

Available from:

National Technical Information Service
U.S. Department of Commerce
5285 Port Royal Road
Springfield, Virginia 22161

Price Printed Copy \$ * ; Microfiche \$4.50

<u>*Pages</u>	<u>NTIS Selling Price</u>	
1-25	\$7.00	For documents over 600 pages, add \$1.50 for each additional 25-page increment.
25-50	\$8.50	
51-75	\$10.00	
76-100	\$11.50	
101-125	\$13.00	
126-150	\$14.50	
151-175	\$16.00	
176-200	\$17.50	
201-225	\$19.00	
226-250	\$20.50	
251-275	\$22.00	
276-300	\$23.50	
301-325	\$25.00	
326-350	\$26.50	
351-375	\$28.00	
376-400	\$29.50	
401-425	\$31.00	
426-450	\$32.50	
451-475	\$34.00	
476-500	\$35.50	
500-525	\$37.00	
526-550	\$38.50	
551-575	\$40.00	
567-600	\$41.50	

MASTER

CHARGE-EXCHANGE AND FUSION REACTION MEASUREMENTS
DURING COMPRESSION EXPERIMENTS WITH NEUTRAL BEAM HEATING
IN THE TOKAMAK FUSION TEST REACTOR

R. Kaita, W.W. Heidbrink, G.W. Hammett, A.A. Chan, A.C. England[†]
H.W. Hendel,^{*} S.S. Medley, E. Nieschmidt,^Δ A.L. Roquemore,
S.D. Scott, J.D. Strachan, G.D. Tait, G. Taylor, C.E. Thomas,[‡]
and K.-I. Wong

Plasma Physics Laboratory, Princeton University
Princeton, New Jersey 08544

ABSTRACT


Adiabatic toroidal compression experiments were performed in conjunction with high power neutral beam injection in the Tokamak Fusion Test Reactor (TFTR). Acceleration of beam ions to energies nearly twice the injection energy was measured with a charge-exchange neutral particle analyzer. Measurements were also made of 2.5 MeV neutrons and 15 MeV protons produced in fusion reactions between the deuterium beam ions and the thermal deuterium and ^3He ions, respectively. When the plasma was compressed, the $d(d,n)^3\text{He}$ fusion reaction rate increased a factor of five, and the $^3\text{He}(d,p)^4\text{He}$ rate by a factor of twenty. These data were simulated with a bounce-averaged Fokker-Planck program, which assumed conservation of angular momentum and magnetic moment during compression. The results indicate that the beam ion acceleration was consistent with adiabatic scaling.

*On leave from RCA David Sarnoff Research Center, Princeton, NJ 08540.

[†]Oak Ridge National Laboratory, Oak Ridge, TN 37831.

[‡]Georgia Institute of Technology, Atlanta, GA 30332.

^ΔIdaho National Engineering Laboratory, Idaho Falls, ID 83415.


DISTRIBUTION OF THIS DOCUMENT IS UNLIMITED

I. Introduction

Adiabatic toroidal compression has been proposed as a means of directly heating tokamak plasmas.¹ The process has been predicted to accelerate beam ions to energies that provide the optimum ratio of fusion reaction rate to plasma drag, thereby avoiding the complexities of excessively high beam injection voltages.¹ The first experiments of this kind were performed in the ATC tokamak,² and the compressional heating of ohmic plasmas in TFTR has been successfully demonstrated.³ Preliminary measurements of the acceleration of beam ions during compression of neutral-beam-heated plasmas were reported recently.⁴ This paper extends that work by providing the details of the experimental and computational procedures used to obtain these results, and includes a more comprehensive set of charge-exchange neutral and fusion-reaction product data under a variety of plasma conditions.

Approximately two megawatts of deuterium neutral beams were injected tangentially into deuterium plasmas at two different plasma densities. The beams were injected for a time interval of either 200 msec or 500 msec immediately preceding compression, and the plasma major radius was subsequently compressed from 3 m to 2.17 m in 15 msec, a time short compared to the collisional relaxation time of the beam ion distribution in the plasma. In some discharges, the beams were kept on during compression, and in others, the major radius was only compressed to 2.58 m.

Fast ion distributions were measured with a horizontally scanning, charge-exchange neutral analyzer (CENA).⁵ Fission chamber and plastic scintillator detectors measured the fusion neutron yield as a function of time.⁶ Prior to beam injection, ^3He was added to the plasma to provide a target for the $^3\text{He}(d,p)\alpha$ reaction. The energetic protons were then detected with silicon surface barrier detectors.⁷

A bounce-averaged Fokker-Planck program⁸ was used to simulate the fast ion slowing-down energy spectra before and after compression. The code first performed the calculation of neutral beam injection prior to compression, and the resulting fast ion distribution function was stored. The plasma profiles were subsequently changed to reflect compression, and the fast ion distribution was correspondingly varied assuming conservation of angular momentum and magnetic moment. The slowing-down spectra were then calculated as this new distribution underwent collisional relaxation. Both the neutron production and the proton yield from the ${}^3\text{He}(d,p)\alpha$ reaction were also calculated with the Fokker-Planck program. The beam ions, accelerated by the compression, were allowed to decelerate by Coulomb drag on the background plasma. The results of the simulations indicate that the time evolution and change in relative magnitude of these fusion product yields due to compression are close to theoretical expectations.

II. Fast Ion Diagnostics

A. Fast Neutral Analyzer Measurements

Two charge-exchange neutral analyzer (CENA) modules were used to measure the slowing-down distribution of beam ions before and after compression. The CENA modules were installed on a movable cart that allowed them to view the plasma along sightlines in the horizontal midplane of TFTR (Figs. 1 and 2). To ensure that fast neutrals would be detected after the plasma was compressed to its final major radius ($R = 2.17$ m), one of the modules was aimed at a tangency radius (distance of closest approach of its sightline to the centerline of TFTR) of 2.19 m.

The CENA modules have a 180-degree "dee-shaped" region of parallel electric and magnetic fields for mass and energy resolution, respectively.

A channel electron multiplier array provides single particle detection capability along the focal plane of the "dee" sector. The microchannel plates in this array are divided into columns for each of the three mass species (hydrogen, deuterium, and tritium), and each column is divided in turn into 75 energy anodes. Approximately half of the 225 available anodes are typically instrumented with amplifiers and pulse-counting electronics, so each mass column has about thirty-five channels for energy analysis. Fast neutral spectra were obtained up to energies of 200 keV.

B. Neutron Measurements

Neutrons from the $d(d,n)$ fusion reaction were measured with a plastic scintillator and with fission chamber detectors. The stilbene scintillator was mounted between toroidal field coils just outside the TFTR vacuum vessel ($R \approx 3.95$ m) at the midplane. The positioning of the detector, together with the fact that a full-energy neutron tends to produce more light in the scintillator than a neutron that is degraded in energy, implies that the signal from the scintillator is dominated by neutrons with energies close to the "virgin" energies. The other detector used in these measurements was a ^{238}U fission chamber detector placed on the floor of TFTR, 1.84 m below the plasma midplane of TFTR, at $R = 4.3$ m. This detector is sensitive to neutrons above 1 MeV, so that neutrons that have lost little energy in scattering are expected to dominate the signal measured by this detector.

During compression, the absolute efficiency (i.e., the ratio of neutron counts to total emission) of these two detectors changes as a function of time as the neutron source moves in major radius. The raw signals from the two detectors during compression are plotted in Fig. 3a. To within 10%, the two signals are identical, indicating that the two detectors

have nearly the same detector efficiency dependence on major radius. Figure 3b shows calibration curves for the two detectors. The scintillator calibration is the detection efficiency as a function of major radius of a scintillator that measures virgin neutrons from a toroidal ring source.⁹ The calibration curve for the ^{238}U detector was obtained by positioning a ^{252}Cf radioactive source inside the vacuum vessel at the toroidal location of the detector, and measuring the count rate as a function of major radius. A more sensitive fission detector (polyethylene-moderated ^{235}U), having a similar sensitivity to radial plasma motion as the ^{238}U detector, but with a detection efficiency nearly independent of energy, was used in this calibration measurement.

It should be noted that although the two calibrations agree to within 10% (Fig. 3a), they both tend to overestimate the sensitivity to radial motion of the plasma. The scintillator calibration curve neglects the contribution of neutrons that reach the detector after scattering off the inner wall or field coils. (The flux of these scattered neutrons is expected to be relatively insensitive to the radial position of the plasma.) Monte Carlo calculations suggest that the scattered flux of neutrons above 1.9 MeV is between 15%¹⁰ and 50%¹¹ of the uncollided flux. The fission detector calibration curve was measured at the toroidal location nearest the detector. During plasma operation, the neutron source has a larger toroidal extent (65 degrees FWHM). The radial sensitivity of the detection efficiency for this extended neutron source is expected to be weaker than measured during the calibration. In our analysis, we have used the scintillator calibration curve (Fig. 3b), but this may overestimate the enhancement to the neutron production by as much as 25%.

C. Proton Measurements

A small amount of ^3He gas was introduced into the deuterium plasma about 250 msec before compression. The 15 MeV protons from the $^3\text{He}(d,p)$ reaction were detected using a silicon surface barrier detector mounted at the bottom of the TFTR vacuum vessel (Fig. 4). The detector was shielded from plasma particles and other fusion products by an 0.18mm stainless steel foil. The collimating apertures of the detector were relatively wide, about 14 degrees (FWHM) in pitch angle. Calculations indicate that the probability of detecting the 15 MeV protons was a factor of one to four greater in the precompressed plasma than in the postcompressed plasma.¹² This is because the proton orbits accessible to the detector originated closer to the magnetic axis, where the bulk of the fusion reactions occur, in the precompressed plasma (Fig. 4).

The calculated proton detection efficiency is more uncertain in TFTR than in previous experiments¹² because the TFTR first wall structures (bellows cover plates) obstruct many of the protons that would otherwise reach the detector, and small uncertainties in the position of the plates result in large uncertainties in the proton flux at the detector. Substantial uncertainties of about 50% are also associated with the fact that the exact distribution in minor radius of the $d\text{-}^3\text{He}$ reactions is not known. The data in Sec. III are corrected to reflect our best estimate of the proton detection, but the comparison of the precompression and postcompression values is only accurate to a factor of two.

III. Experimental Results

Figure 5a shows the fast ion slowing-down spectra before and after compression for a low density plasma. The solid lines in Fig. 5a and in all subsequent plots are derived from Fokker-Planck calculations, which

will be described in Sec. IV. The injection energy was 82 keV, and the neutral beams were turned off when the compression occurred at 2.5 sec. These data were obtained during one shot using a tangentially viewing CENA module, averaged over 10 msec.

The data indicate that many ions were accelerated from 80 keV up to a maximum of 150 keV. For reasons to be discussed in Sec. IV, the highest energy expected from a compression ratio of 1.38 is 158 keV. The rise in the absolute magnitude of the fast neutral flux is thought to be the higher neutral density due to enhanced recycling from the inner wall, which served as a limiter for the postcompression plasma. Before compression, the limiter was a structure with vertically movable blades at a fixed toroidal location of about 72 degrees from the CENA module sightline.

As a result of compression, the neutron yield increased by a factor of 5.5 above the steady-state, precompression value (Fig. 5b). On this figure and on all subsequent plots of fusion product results, the dashed curves are derived from calculations which will be discussed in Sec. IV. Because of the high signal levels, statistical errors are insignificant on the scale of the figure. However, the detector calibration changes as the plasma is compressed, and the representative error bar at the peak neutron flux on this and subsequent figures reflects the uncertainty due to this systematic calibration error.

The increase in the neutron yield is due both to the rise in the deuterium target density, which adiabatic scaling predicts to be a factor of 1.9, and to the acceleration of the beam ions, since the $d(d,n)$ reactivity (σv) increases by a factor of 3.2 when the deuteron energy goes from 80 keV to 150 keV. Subsequently, the neutron emission decays as the beam ions undergo Coulomb relaxation.

The time evolution of the proton yield (Fig. 5c) is similar, except that the rise is much larger. This factor of ten to forty is due to the steeper energy dependence of the ${}^3\text{He}(d,p)$ fusion cross section (σ) which is ten times greater at 150 keV than at 80 keV. Prior to compression, the emission is nearly constant, indicating that the ${}^3\text{He}$ density reached a steady state. Following compression, the decay is more rapid than for the neutron emission, since the ${}^3\text{He}(d,p)\alpha$ cross section has a much stronger energy dependence. The fast ion, neutron, and proton measurements for a higher density plasma [$n(e) \approx 2.3 \times 10^{19} \text{ m}^{-2}$], with a 12% lower electron temperature (2.8 keV), are shown in Fig. 6. The most noticeable difference is the faster decay rate of the fusion products after compression, which is consistent with the higher collisionality in this plasma.

For neutral beam injection throughout the compression phase, the results of the three measurements are depicted in Fig. 7. The density in this case was comparable to the first condition discussed [$n(e) \approx 1.3 \times 10^{19} \text{ m}^{-2}$]. The similarity between the fast neutral and fusion product measurements for the two low density plasmas shows that the signals are dominated by the beam ions accelerated by compression to high energy, rather than the 82 keV ions that continue to be injected.

The effect of weaker compression ($C = 1.12$) on the fast ion distribution was studied by compressing the plasma in 15 msec into the center of the TFTR vacuum vessel, and then allowing the plasma to undergo "free expansion" in minor radius until contact with the limiter was restored. For this case (Fig. 8), the beams were turned off prior to compression, and the electron density was fairly low [$n(e) \approx 1.5 \times 10^{19} \text{ m}^{-2}$]. During free expansion, the fusion emission increased only slightly, indicating that for this rate of compression, the acceleration is nearly balanced by Coulomb drag.

In contrast to the full compression cases, the 15 MeV proton detection efficiency for free expansion plasmas is calculated to be a factor of two higher in the postcompression phase than the precompression phase. However, uncertainties in the $d\text{-}^3\text{He}$ emission profile, and in the positioning of the TFTR bellows cover plates, once again make the comparison of the $d\text{-}^3\text{He}$ emission levels before and after compression accurate only to within a factor of two.

IV. Bounce-Averaged Fokker-Planck Simulations

A bounce-averaged Fokker-Planck program was used to simulate the slowing-down spectra and the fusion product yields before and after compression. The Boltzmann equation was solved for the ion distribution function during neutral beam injection up to the time of compression, at which point the calculation was terminated and the distribution function stored.

Since the compression time (~ 15 msec) is much shorter than the collision time (~ 150 msec) for the beam ions, it is assumed that the angular momentum of the beam ions about the major axis ($R \cdot v_\phi \simeq R \cdot v_{||}'$) and the magnetic moment ($\mu = mv_\perp^2/2B$) are invariant quantities. The energy of an ion after compression should therefore be

$$E' = E_{||}' + E_{\perp}' = C^2 \cdot E_{||} + C \cdot E_{\perp} \quad (1)$$

The unprimed and primed quantities are the values of parameters before and after compression respectively, and the compression ratio (C) equals R/R' .

Before compression, the ion energy distribution function from the tangential analyzer (Fig. 5a) cuts off at the injection energy of 82 keV. It is expected that these tangentially injected ions do not undergo

appreciable pitch angle scattering before they are lost as charge-exchange neutrals, and thus will experience the maximum C^2 acceleration predicted for ions moving exactly along the magnetic field. The observation of fast ions up to 150 keV immediately after compression ($C = 1.38$) appears to confirm this scenario.

To simulate the data accurately, the proper experimental geometry before and after compression had to be included in the code. Since the charge-exchange analyzer viewed a chord integral of neutrals coming from ions with a range of pitch angles, the acceleration experienced by the ions below the injection energy was expected to vary. Furthermore, the analyzer sightline relative to the plasma also changed with major radius during compression, leading to the distortion of the shape of the distribution after compression evident in Fig. 5a. The Fokker-Planck code was used to follow the ion distribution in time as a function of energy, pitch angle, and minor radius before compression. This distribution was then saved in a disk file as an intermediate step, and it was read when the code was run to simulate the discharge after compression. For this part of the calculation, the compression ratio (C) was used to scale the changes in the background plasma temperature and density profiles.

Each of the two beamlines installed for this phase of TFTR operation consisted of three ion sources which injected at different tangency radii. Since two of the six sources were used in the compression experiments, their injection angles and acceleration voltages were simulated by repeating the deposition calculation for each source to obtain the total initial beam ion distribution in the plasma. The program also included the usual effects of classical collisional slowing down, energy diffusion and pitch angle scattering, and charge-exchange loss. The long collisional relaxation

time of the beam ions relative to the compression time allowed us to assume instantaneous compression in this model.

Contour plots in velocity space before and after compression are shown in Figs. 9a and 9b, respectively. The plasma was divided into ten evenly distributed radial shells for this calculation, and these plots were obtained for a central shell. The ordinate corresponds to the perpendicular velocity, and the abscissa corresponds to parallel velocity. There is a factor of ten between each contour, and the "trapping boundaries" are evident at $v_{||} / v_{\perp} \approx \pm 0.2$.

Since the beams have reached equilibrium in the precompression contour plot (Fig. 9a), there is both an enhancement around the injection energy as well as a spread in the beam velocity distribution due to energy diffusion and pitch-angle scattering. After compression, the velocities of all of the ions increase. The postcompression contour plot (Fig. 9b) shows a distortion in the direction of increasing parallel velocity. This is because ions with parallel velocity are accelerated by a factor equal to the compression ratio, whereas those with perpendicular velocity only see a change proportional to the square root of this ratio.

The fits to the charge-exchange spectra discussed in the preceding section were obtained by integrating the product of the calculated fast ion distribution function and a calculated neutral density profile using a one-dimensional model¹³ for its profile shape. Since the variation of the neutral density in time during compression was not known, the absolute magnitude of the charge-exchange signal could not be calculated. However, the shapes of the predicted spectra (solid lines in Figs. 5a, 6a, and 7a) are in reasonable agreement with the experimental data, so the energy gained by fast ions during compression and their subsequent decay appear to be consistent with classical expectations.

The fusion neutron yield was also calculated concurrently by the Fokker-Planck code, and the predictions are compared with experiment in Figs. 5b, 6b, and 7b. The absolute value of the calculated yield before compression, assuming 2.1 MW deuterium beams in a 100% deuterium plasma, exceeded the data by a factor of two. Since relative changes in the yield with compression were of primary interest, however, and considering the uncertainties in the neutron detector calibration, deuterium concentration, and neutral beam species ratios and deposition profiles, the code results were normalized to the precompression level.

The electron temperature did not rise in accordance with adiabatic scaling, but the increase was about 30% lower on average than expected. The reason for the anomalous electron behavior is not yet understood,³ and the temperatures measured with the electron cyclotron emission (ECE) radiometer diagnostic were used in the Fokker-Planck program instead of the expected values for postcompression plasmas.

In the simulation, the fast ion distribution function was compressed and allowed to undergo Coulomb relaxation for 100 msec. The electron and ion temperatures and the electron densities were varied by $\pm 10\%$ to reflect uncertainties in the measurements of the background plasma parameters. Their effects in setting upper and lower limits on the predicted fusion reactions are shown by the dashed lines on the plots of neutron yield and proton production. The beams continued to fuel the plasma in the case where they remained on during compression (Fig. 7b), and the highest peak neutron yield of $6 \times 10^{14} \text{ sec}^{-1}$ was achieved under these conditions.

The total proton yield from the ${}^3\text{He}(d,p)\alpha$ reaction was also simulated at the same time that the neutron and fast neutral predictions were being calculated. The target plasma for this part of the simulation was assumed

to be entirely helium since its actual concentration was not known, and its magnitude was normalized to the precompression measurement. The ${}^3\text{He}(d,p)\alpha$ fusion reactivity increases by a factor of 14 as the deuteron energy varies from 80 keV to 150 keV, and this dramatic rise in the reaction rate due to compression is evident in the data (Figs. 5c, 6c, and 7c). Although the code results do not simulate as large an increase, they are reasonable considering the uncertainties in both the calculations and the data.

V. Conclusions

Fast ion measurements during adiabatic toroidal compression in TFTR have shown that beam ions injected at 80 keV are accelerated to energies up to 150 keV after compression, in accordance with expectations for a compression ratio of 1.38. Using the assumptions of conservation of angular momentum and magnetic moment to vary the beam ion distribution in a bounce-averaged Fokker-Planck program, the calculated fast ion slowing-down distributions agreed with the shape of the spectra from charge-exchange measurements. The measured neutron production and the proton yield from the ${}^3\text{He}(d,p)\alpha$ reaction were also simulated with the Fokker-Planck code, and its predictions for their relative changes with time are generally in agreement with experiment.

Acknowledgments

The authors wish to express their gratitude to the many physicists, engineers, and technicians who were responsible for the construction and successful operation of TFTR and the neutral beam injection systems. We would also like to thank Dr. R. Goldston for helpful discussions concerning the Fokker-Planck simulations. This work was supported by U.S. Department of Energy Contract DE-AC02-76-CHO-3073.

References

- ¹H.P. Furth and S. Yoshikawa, Phys. Fluids 13, 2593 (1970).
- ²R.A. Ellis, H.P. Eubank, R. Goldston, R.R. Smith, and T. Nagashima, Nucl. Fusion 16, 524 (1976).
- ³G. Tait, J. Bell, M.G. Bell, M. Bitter, W.R. Blanchard, et al., in Plasma Physics and Controlled Nuclear Fusion Research (Proc. 10th Int. Conf. London, 1984) Vol. 1, IAEA, Vienna (1985) 141.
- ⁴K.-L. Wong, M. Bitter, G. Hammett, W. Heidbrink, H. Hendel, et al., Phys. Rev. Lett. 55, 2587 (1985).
- ⁵S.S. Medley, Princeton Plasma Physics Laboratory Report No. PPPL-1770 (1980); also A.L. Roquemore, G. Gammel, G.W. Hammett, R. Kaita, and S.S. Medley, Rev. Sci. Instrum. 56, 1120 (1985).
- ⁶J.D. Strachan, P.L. Colestock, S.L. Davis, D. Eames, P.C. Efthimion, et al., Nucl. Fusion 21, 67 (1981); also H.W. Hendel, K. Matsuoka, and L.E. Samuelson, Proc. Fourth ASTM-EURATOM Symp. on Reactor Dosimetry CONF-820321/V2, Nat. Bureau of Standards, Washington (1982) 94.
- ⁷R.E. Chrien and J.D. Strachan, Phys. Fluids 26, 1953 (1983).
- ⁸J.G. Cordey, Nucl. Fusion 16, 499 (1976); also R.J. Goldston, Ph. D. Thesis, Princeton University (1977).
- ⁹G. Zankl, J. Strachan, R. Lewis, W. Pettus, and J. Schmotzer, Nucl. Instrum. Methods 185, 321 (1981).
- ¹⁰J.V. Foley, M.S. Thesis, Princeton University (1985).
- ¹¹L.P. Ku, J.G. Kolibal, and S.L. Liew, Princeton Plasma Physics Laboratory Report No. PPPL-2244 (1985).
- ¹²W. Heidbrink and J. Strachan, Rev. Sci. Instrum. 56, 501 (1985).
- ¹³S. Tamor, J. Comput. Phys. 40, 104 (1981).

Figure Captions

- Fig. 1. Plan view of TFTR, showing the layout of the CENA array. (PPPL-85X1628)
- Fig. 2. Elevation view of TFTR, showing the support structure for CENA array. The approximate positions of the plasma before and after compression are indicated schematically by the two smaller circles within the vacuum vessel. (PPPL-85X1627)
- Fig. 3. a) Time evolution of the signal from a plastic scintillator (solid line) and from a fission detector (points with error bars) during major radius compression. b) Neutron detection efficiency as a function of major radius for the plastic scintillator (solid line) and for the fission detector (error bars). (PPPL-85X1466)
- Fig. 4. Poloidal projection of a 15 MeV proton orbit accessible to the silicon surface barrier detector at the bottom of TFTR for the precompression plasma and for the postcompression plasma. (PPPL-86X0105)
- Fig. 5. a) Slowing-down spectra for 2.1 MW deuterium beams in a 3.9 T, 445 kA deuterium plasma. The spectra shown on this and all subsequent figures were obtained using a tangentially viewing charge-exchange neutral analyzer (CENA). Data before compression are displayed with open circles with error bars (2.485 sec), and data after compression are depicted with error bars (2.515 sec) and closed circles with error bars (2.535 sec). b) Neutron production for this plasma. c) Proton yield from the ${}^3\text{He}(d,p)\alpha$ reaction for this plasma. (PPPL-86X0108)

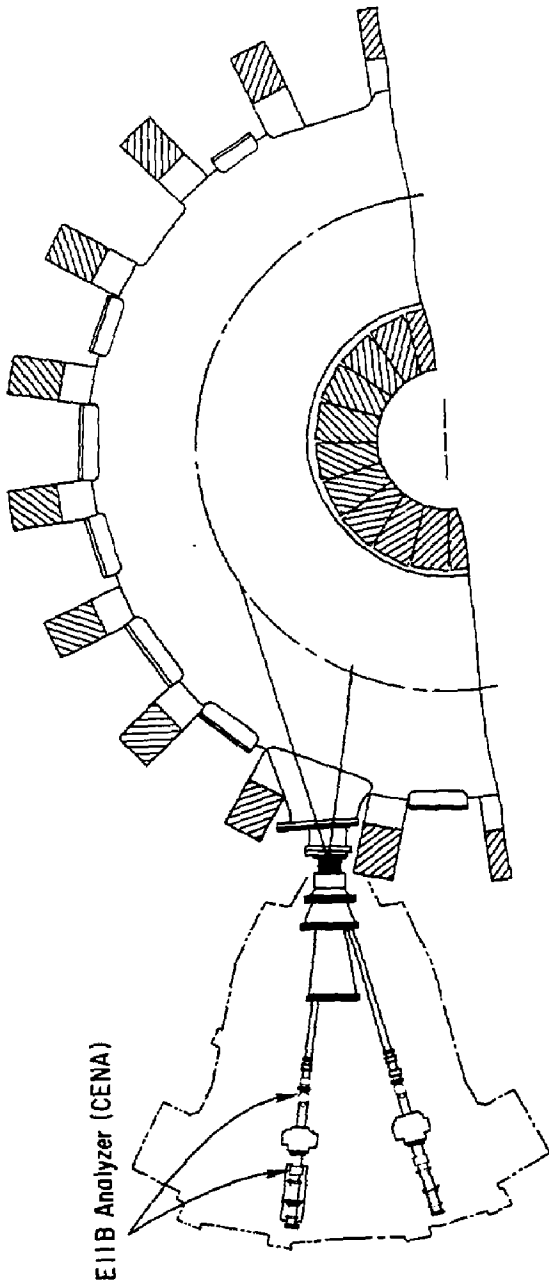
Fig. 6. Slowing-down spectra from the tangentially viewing CENA (a), neutron production (b), and proton yield from the ${}^3\text{He}(d,p)\alpha$ reaction (c) for a plasma similar to Fig. 5 (3.3 T, 441 kA), but with higher density [$n(e) \approx 2.3 \times 10^{19} \text{ m}^{-2}$]. (PPPL-86X0106)

Fig. 7 Slowing-down spectra from the tangentially viewing CENA (a), neutron production (b), and proton yield from the ${}^3\text{He}(d,p)\alpha$ reaction (c) for a plasma similar to Fig. 5 (3.3 T, 444 kA), but with the beams remaining on throughout compression (until 2.6 sec). (PPPL-86X0107)

Fig. 8 Slowing-down spectra from the tangentially viewing CENA (a), neutron production (b), and proton yield from the ${}^3\text{He}(d,p)\alpha$ reaction (c) for a plasma similar to Fig. 5 (3.5 T, 590 kA), but with weaker compression ($C = 1.12$), followed by "free expansion" in minor radius. (PPPL-86X0109)

Fig. 9 a) Contour plot of ion distribution function before compression, generated by bounce-averaged Fokker-Planck program. The axes are normalized to $v_0 = \sqrt{2m \cdot 200 \text{ keV}}$, and each contour is separated from the next by an order of magnitude. b) Contour plot of ion distribution function after compression, generated by the same Fokker-Planck program. (PPPL-86X0110)

#85 X 1628



E11B Analyzer (CENA)

Fig. 1

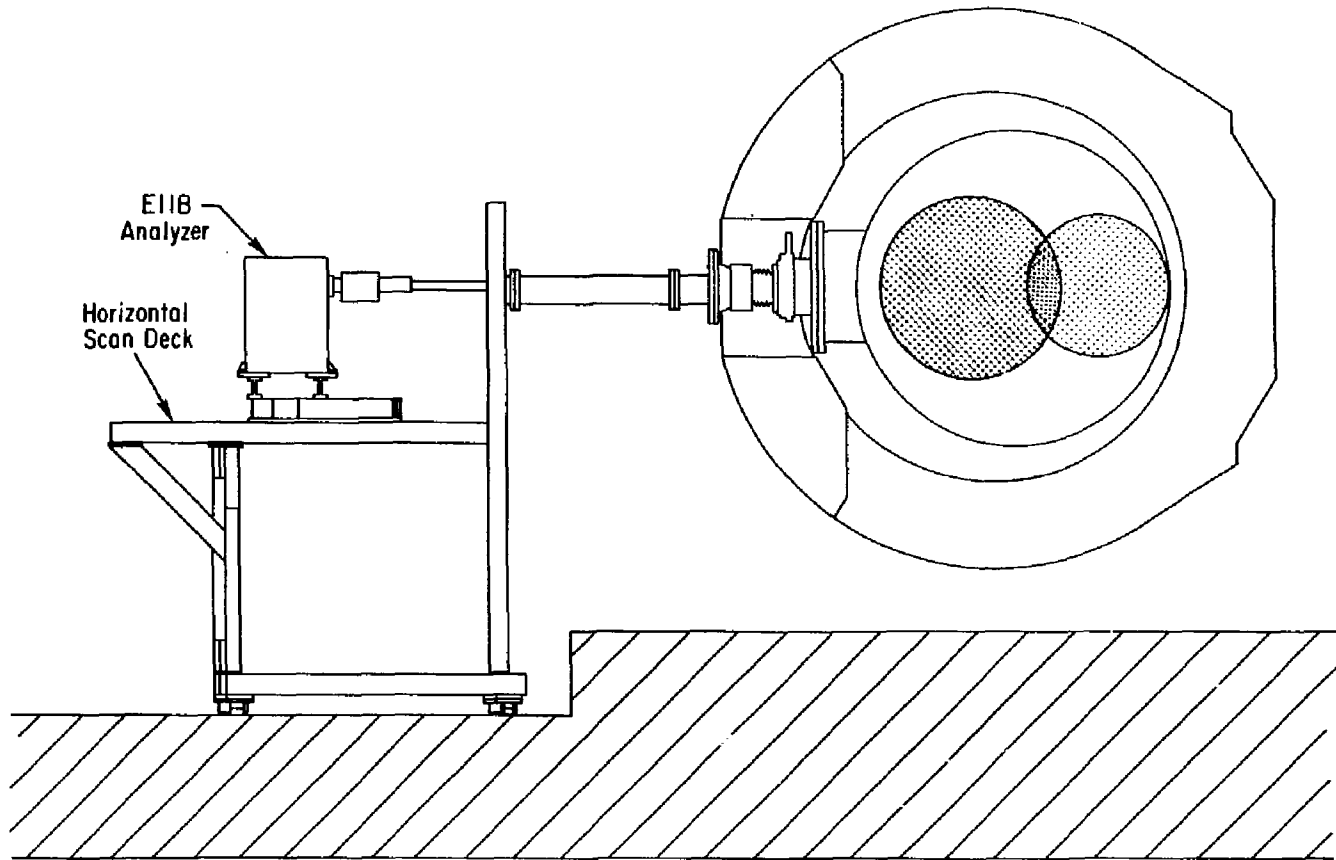


Fig. 2

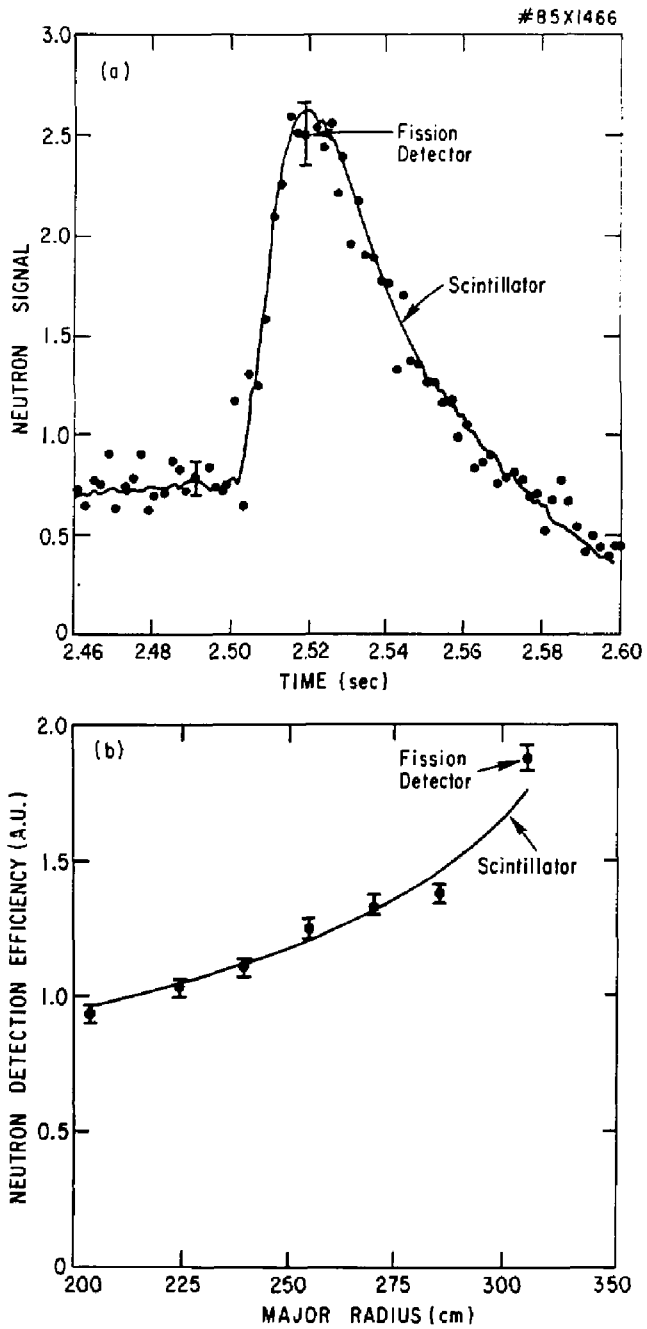


Fig. 3

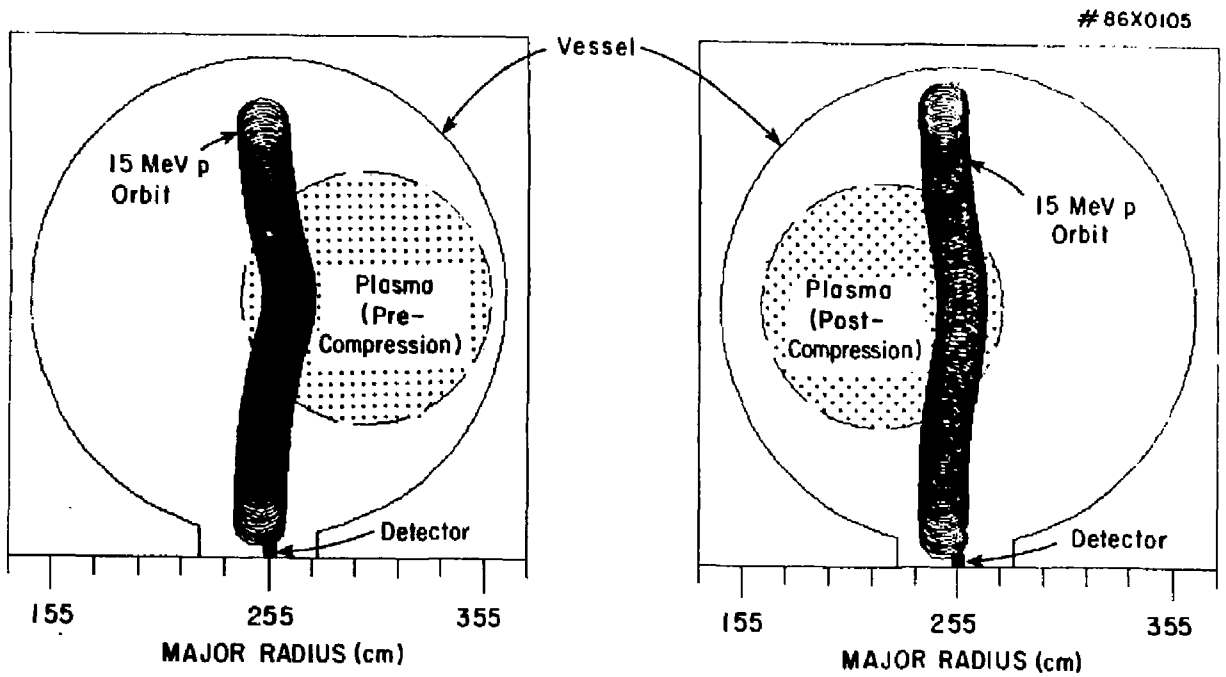


Fig. 4

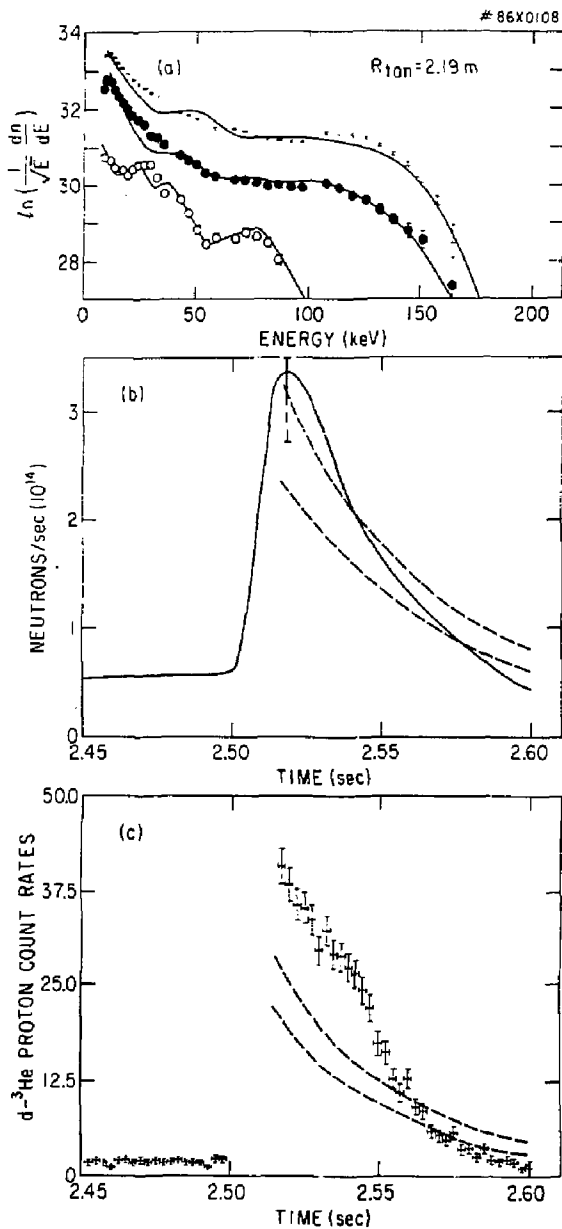


Fig. 5

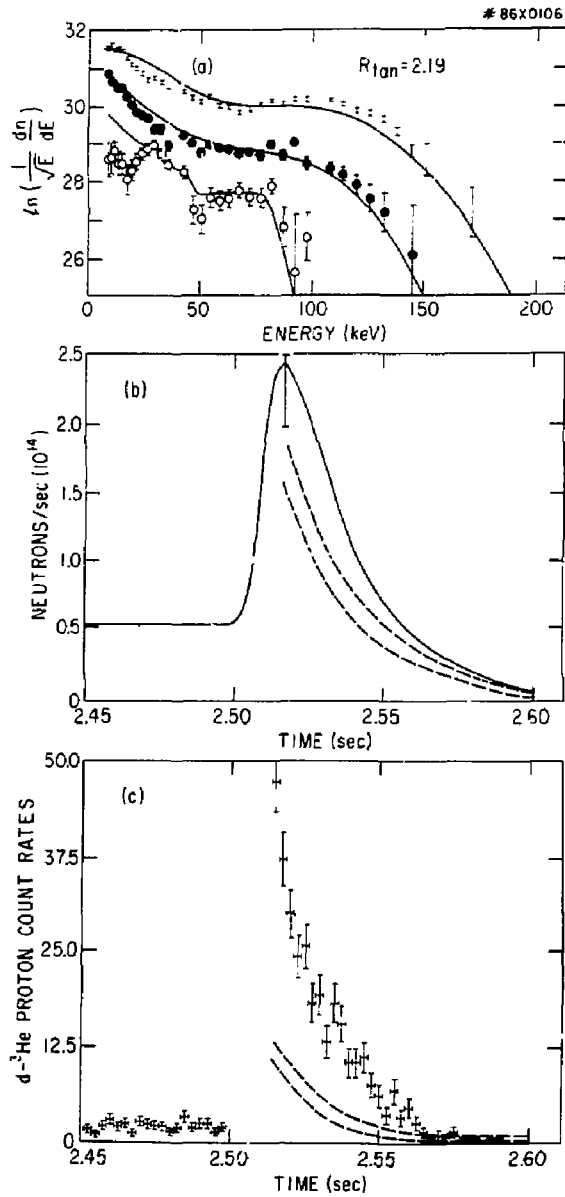


Fig. 6

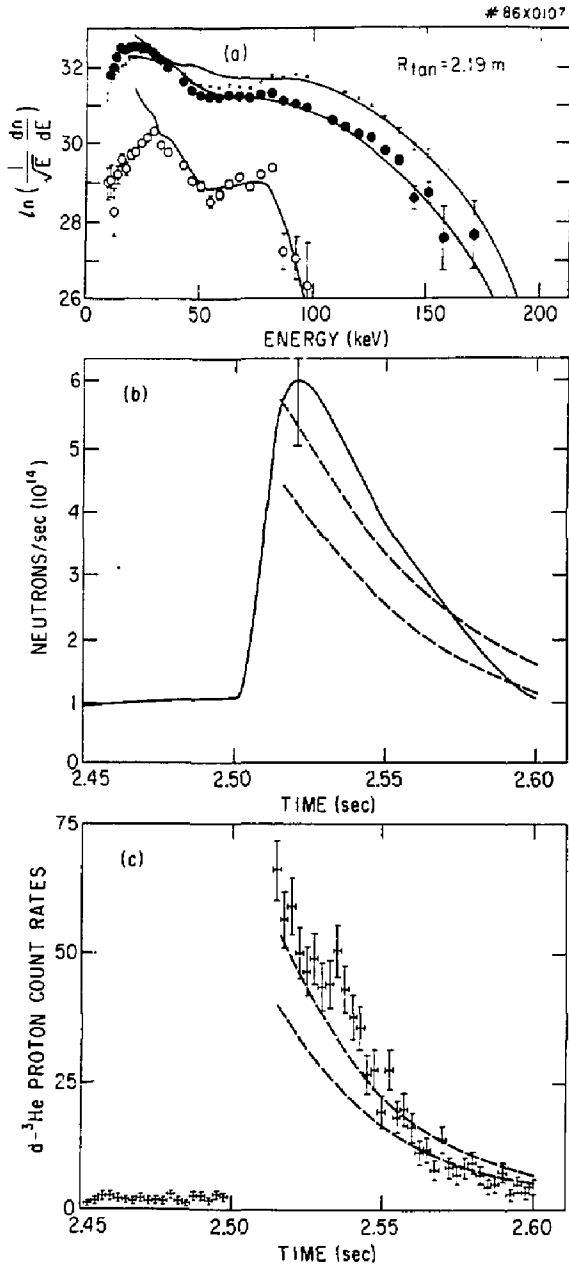


Fig. 7

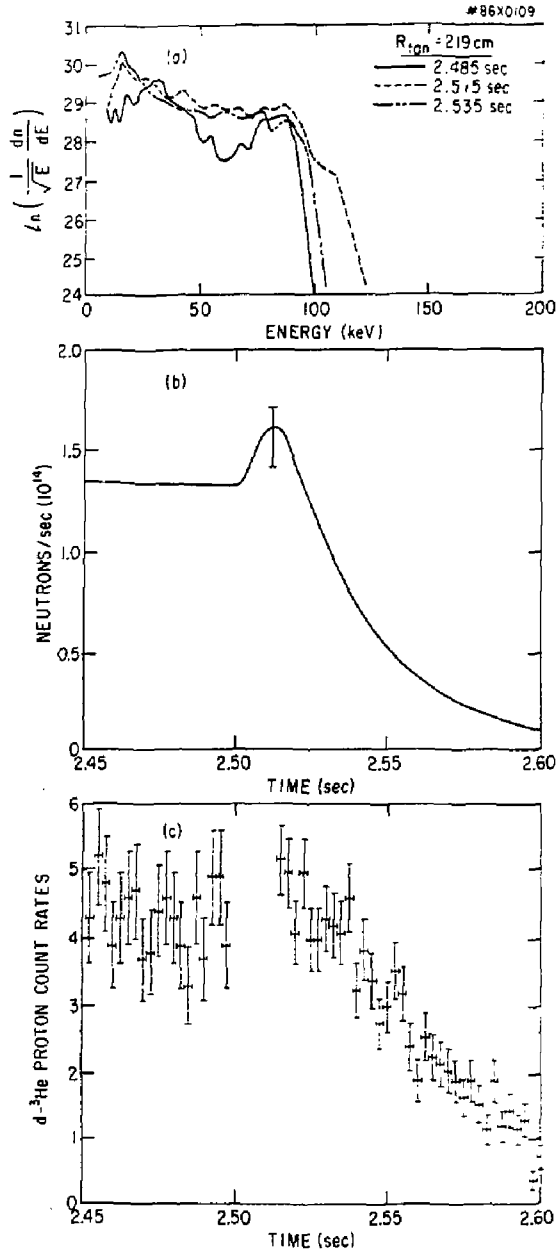


Fig. 8

#86X0110

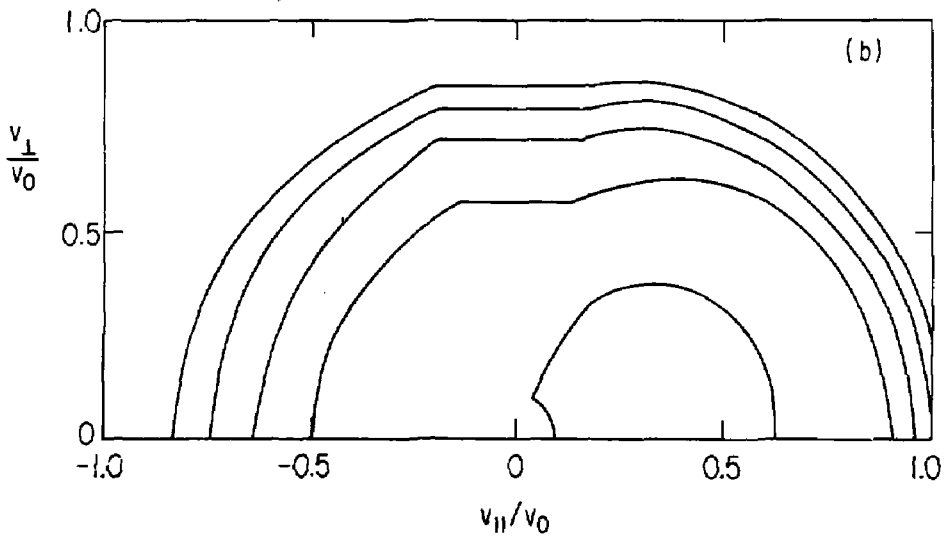
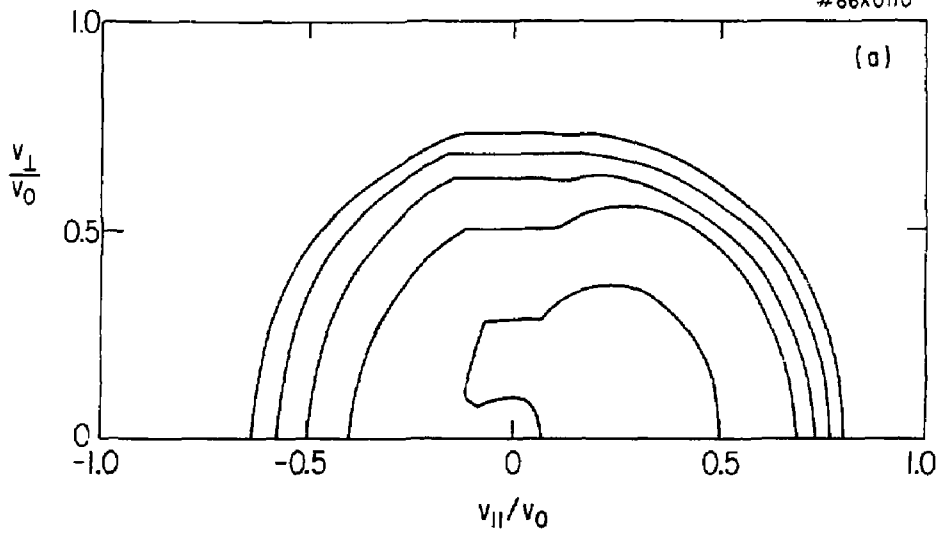


Fig. 9

EXTERNAL DISTRIBUTION IN ADDITION TO UC-20

Plasma Res Lab, Austr Nat'l Univ, AUSTRALIA
Dr. Frank J. Paoloni, Univ of Wollongong, AUSTRALIA
Prof. I.R. Jones, Flinders Univ., AUSTRALIA
Prof. M.H. Brennan, Univ Sydney, AUSTRALIA
Prof. P. Cap, Inst Theo Phys, AUSTRIA
Prof. Frank Verheest, Inst theoretische, BELGIUM
Dr. D. Palumbo, Dg XII Fusion Prog, BELGIUM
Ecole Royale Militaire, Lab de Phys Plasmas, BELGIUM
Dr. P.H. Sakanaka, Univ Estadual, BRAZIL
Dr. C.R. James, Univ of Alberta, CANADA
Prof. J. Teichmann, Univ of Montreal, CANADA
Dr. H.M. Skarsgard, Univ of Saskatchewan, CANADA
Prof. S.R. Sreenivasan, University of Calgary, CANADA
Prof. Tudor W. Johnston, INRS-Energie, CANADA
Dr. Hannes Barnard, Univ British Columbia, CANADA
Dr. M.P. Bachynski, MPB Technologies, Inc., CANADA
Chalk River, Nucl Lab, CANADA
Zhengwu Li, SW Inst Physics, CHINA
Library, Tsing Hua University, CHINA
Librarian, Institute of Physics, CHINA
Inst Plasma Phys, Academia Sinica, CHINA
Dr. Peter Lukac, Komenskeho Univ, CZECHOSLOVAKIA
The Librarian, Culham Laboratory, ENGLAND
Prof. Schatzman, Observatoire de Nice, FRANCE
J. Radet, CEN-BP6, FRANCE
AM Dupas Library, AM Dupas Library, FRANCE
Dr. Tom Mual, Academy Bibliographic, HONG KONG
Preprint Library, Cent Res Inst Phys, HUNGARY
Dr. R.K. Chhajlani, Vikram Univ. INDIA
Dr. B. Dasgupta, Saha Inst, INDIA
Dr. P. Kaw, Physical Research Lab, INDIA
Dr. Phillip Rosenau, Israel Inst Tech, ISRAEL
Prof. S. Cuperman, Tel Aviv University, ISRAEL
Prof. G. Rostagni, Univ Di Padova, ITALY
Librarian, Int'l Ctr Theo Phys, ITALY
Miss Clelia De Palo, Assoc EURATOM-ENEA, ITALY
Biblioteca, del CNR EURATOM, ITALY
Dr. H. Yamato, Toshiba Res & Dev, JAPAN
Direc. Dept. Lg. Tokamak Dev, JAERI, JAPAN
Prof. Nobuyuki Inoue, University of Tokyo, JAPAN
Research Info Center, Nagoya University, JAPAN
Prof. Kyoji Nishikawa, Univ of Hiroshima, JAPAN
Prof. Sigeru Mori, JAERI, JAPAN
Prof. S. Tanaka, Kyoto University, JAPAN
Library, Kyoto University, JAPAN
Prof. Ichiro Kawakami, Nihon Univ, JAPAN
Prof. Satoshi Itoh, Kyushu University, JAPAN
Dr. D.I. Choi, Adv. Inst Sci & Tech, KOREA
Tech Info Division, KAERI, KOREA
Bibliothek, Fom-Inst Voor Plasma, NEETHERLANDS
Prof. B.S. Liley, University of Waikato, NEW ZEALAND
Prof. J.A.C. Cabral, Inst Superior Tecn, PORTUGAL
Dr. Octavian Petrus, ALI OJZA University, ROMANIA
Prof. M.A. Hellberg, University of Natal, SO AFRICA
Dr. Johan de Villiers, Plasma Physics, Nucco, SO AFRICA
Fusion Div. Library, JEN, SPAIN
Prof. Hans Wilhelmson, Chalmers Univ Tech, SWEDEN
Dr. Lennart Stenflo, University of UMEA, SWEDEN
Library, Royal Inst Tech, SWEDEN
Centre de Recherchesen, Ecole Polytech Fed, SWITZERLAND
Dr. V.T. Tolok, Kharkov Phys Tech Ins, USSR
Dr. D.D. Ryutov, Siberian Acad Sci, USSR
Dr. G.A. Elisseev, Kurchatov Institute, USSR
Dr. V.A. Glukhikh, Inst Electro-Physical, USSR
Institute Gen. Physics, USSR
Prof. T.J.M. Boyd, Univ College N Wales, WALES
Dr. K. Schindler, Ruhr Universitat, W. GERMANY
Nuclear Res Estab, Julich Ltd, W. GERMANY
Librarian, Max-Planck Institut, W. GERMANY
Bibliothek, Inst Plasmaforschung, W. GERMANY
Prof. R.K. Janev, Inst Phys, YUGOSLAVIA